RSC Advances

PAPER

Cite this: *RSC Adv.*, 2024, **14**, 12966

A surface-independent bioglue using photo-crosslinkable benzophenone moiety†

Yue Shi,[a] Xuelian Tao,[b] Ping Du,[b] Paul Pasic,[c] Lars Esser,[c] Hsien-Yeh Chen,[d] Helmut Thissen[c] and Peng-Yuan Wang *[a]

Surface coating technology is broadly demanded across various fields, including marine and biomedical materials; therefore, a facile and versatile approach is desired. This study proposed an attractive surface coating strategy using photo-crosslinkable benzophenone (BP) moiety for biomaterials application. BP-containing "bioglue" polymer can effectively crosslink with all kinds of surfaces and biomolecules. Upon exposure to ultraviolet (UV) light, free radical reaction from the BP glue facilitates the immobilization of diverse molecules onto different substrates in a straightforward and user-friendly manner. Through either one-step, mixing the bioglue with targeted biomolecules, or two-step methods, pre-coating the bioglue and then adding targeted biomolecules, polyacrylic acid (PAA), cyclic RGD-containing peptides, and proteins (gelatin, collagen, and fibronectin) were successfully immobilized on substrates. After drying the bioglue, targeted biomolecules can still be immobilized on the surfaces preserving their bioactivity. Cell culture on biomolecule-immobilized surfaces using NIH 3T3 fibroblasts and human bone marrow stem cells (hBMSCs) showed significant improvement of cell adhesion and activity compared to the unmodified control in serum-free media after 24 hours. Furthermore, hBMSCs on the fibronectin-immobilized surface showed an increased calcium deposition after 21 days of osteogenic differentiation, suggesting that the immobilized fibronectin is highly bioactive. Given the straightforward protocol and substrate-independent bioglue, the proposed coating strategy is promising in broad-range fields.

Received 11th March 2024
Accepted 9th April 2024

DOI: 10.1039/d4ra01866d

rsc.li/rsc-advances

1. Introduction

Surface coatings are crucial to a wide range of biomedical applications, including implants, sensors, and biomedical devices, which require biological functions at the biointerfaces. Functionalizing surfaces using substrate-independent coating methods has garnered increasing attention in both laboratory and industrial settings. Several techniques have been developed so far, such as polyphenol-based coatings, aminomalononitrile (AMN)-based coatings, plasma-based coatings,[1] and chemical vapor deposition (CVD)-based coatings.[2,3]

Polydopamine (PDA) is the classic polyphenol-based material inspired by mussel's adhesion.[4] PDA-based coating is a straightforward, one-pot polymerization process.[5] The strong adhesion properties and chemical versatility have rendered PDA a powerful "glue" in diverse fields, including energy, environmental, catalytic, and biomedical applications.[6,7] PDA serves not only as a mediator for biomolecule coatings on the nanoscale but also as a self-assembled polymer for fabricating nanoparticles and capsules.[8,9] PDA-modified coatings have been used in tissue engineering, bioimaging, biosensing, drug delivery, photothermal therapy, antimicrobial coatings, *etc.*[10,11] In the meantime, other polyphenol materials such as poly(tannic acid), poly(norepinephrine), poly(gallic acid) shows similar potentials as adhesives and applications in optical materials, sensors, and biomedical materials.[12–14]

Hydrogen cyanide (HCN)-derived polymers such as AMN have been studied for decades in prebiotic chemistry; however, HCN-based coating was only discovered in 2015.[15] AMN-based coatings have several advantages, such as ease-to-produce and biocompatibility, making them a favorable material in biomedical applications.[16,17] By choosing different co-polymers, AMN-based coatings has shown versatile properties, including antifouling, antibacterial,[18] low foreign body reaction (FBR)[19] and improving osteogenic differentiation of human mesenchymal stem cells (hMSCs).[20]

Chemical vapor deposition (CVD) and plasma polymerization offer solvent-free options on a wide range of substrates.[21] In these cases, thin films can be formed on substrates *via* gas-phase precursor reactions initiated by either temperature (*e.g.*, CVD) or additional energy (*e.g.*, plasma). Both techniques are

[a]*Oujiang Laboratory, Key Laboratory of Alzheimer's Disease of Zhejiang Province, Institute of Aging, Wenzhou Medical University, Wenzhou, Zhejiang 325000, China. E-mail: py.wang@ojlab.ac.cn*

[b]*Shenzhen Key Laboratory of Biomimetic Materials and Cellular Immunomodulation, Shenzhen Institute of Advanced Technology, Chinese Academy of Sciences, Shenzhen, Guangdong 518055, China*

[c]*CSIRO Manufacturing, Research Way, Clayton, Victoria 3168, Australia*

[d]*Department of Chemical Engineering, National Taiwan University, Taipei, Taiwan*

† Electronic supplementary information (ESI) available. See DOI: https://doi.org/10.1039/d4ra01866d

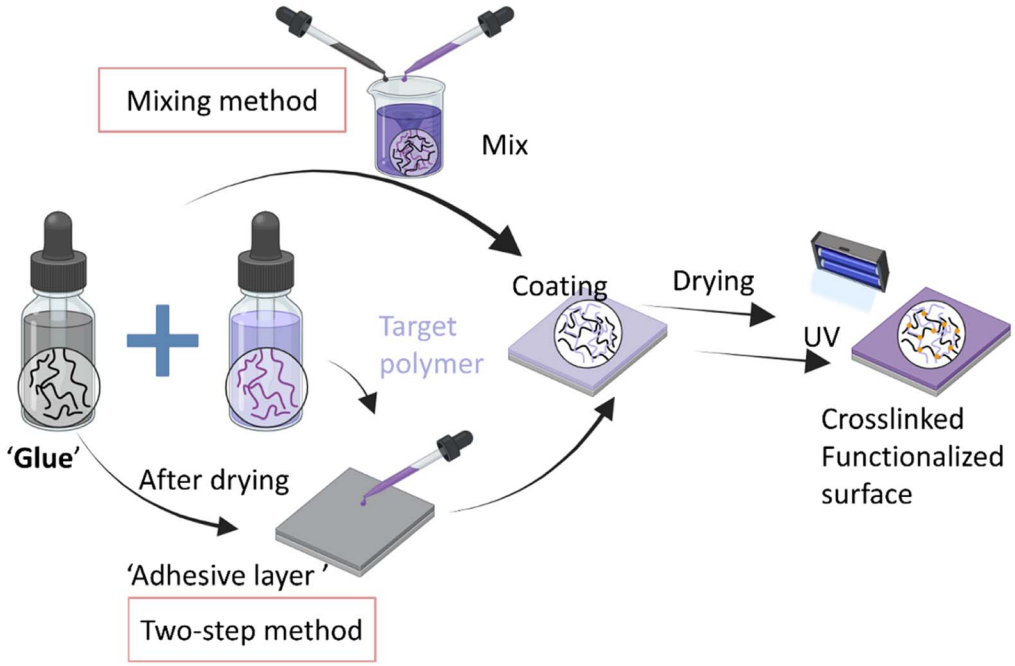

Scheme 1 Schematic illustration of the experiment design: utilizing a glue polymer for robust immobilization of targeted functional groups onto diverse substrates. Two methods were applied in this study. The mixing method involves blending the target polymer with the glue polymer before coating process. The second method, referred to as the 'two-step method,' entails the initial formation of an adhesive layer using the glue polymer, followed by the deposition of the target polymer film on top. After UV exposure, the crosslinking reaction induced by the glue polymer can immobilize targeted functional groups onto the substrates.

widely used in modern industries covering electronics, surface modification, and biomedical applications.

However, the abovementioned methods also have their own disadvantages. For instance, solution-based coatings require additional steps for termination and by-product removal, while vapor-based coatings need equipment and have challenges for complex shapes. This study proposed a straightforward coating methodology employing a "glue polymer", incorporating UV light-curable motifs (*i.e.*, benzophenone groups) within a biocompatible poly *t*-butyl acrylate backbone. This polymer is designed to immobilize various biomolecules onto different types of substrates readily. While traditional methods may require adjustment for each type of substrate or polymer, the involvement of this polymer offers a simple and consistent approach to coating diverse molecules onto various substrates.

This versatile method is substrate-independent and allows surface coating in the air. The "glue polymer" can be combined with other compounds, such as polymers containing targeted functional groups, to co-deposit on the substrate or serve as an adhesive layer facilitating the immobilization of targeted polymers (Scheme 1). The novelty of this coating methodology lies in its operational simplicity and broad applicability to various substrates and polymers. It requires no sophisticated equipment or reaction conditions yet enables the functionalization of a wide range of polymers onto different substrates using the same method.

In this proof-of-concept study, polyacrylic acid (PAA) polymer, cyclic RGD-containing peptides, and proteins (gelatin, collagen, and fibronectin) were immobilized using the "glue polymer". The stability and biofunctions of the coatings were analyzed using surface characterization and mammalian cell cultures. This study provides a new option for surface coating and benefits biomaterials and tissue engineering.

2. Results

2.1. The BP glue polymer

The "glue polymer", *t*-butyl acrylate/*N*-benzophenone acrylate, (poly(BA_{95}–BPA_5)) copolymers, was synthesized using the reversible addition–fragmentation chain transfer (RAFT) polymerization, a well-controlled process that is known for its ability to render narrow polydispersity (Scheme 2). The obtained "glue polymer" had a M_n of *ca.* 25 100 and M_w/M_n of 1.23. The component composition ratio calculated based on the ^{1}H NMR spectrum (Fig. S1†) showed 5.2% BPA in the copolymer, which aligned well with the initial monomer feeding ratios (*t*-BA : BPA 95 : 5 molar ratio). To test the ability of the BP "glue polymer" for surface coating on different substrates, polystyrene (PS), glass slides, and Ti substrates, representing polymer, inorganic, and metal substrates, were tested.

Water contact angle (WCA) measurement and X-ray photoelectron spectroscopy (XPS) were used to characterize the modified surfaces. The surface wettability of different substrates was almost the same after coating (WCA $\sim$ 88°, Fig. 1A). High-resolution C 1s scan and a wide scan showed nearly identical spectrum and similar chemical compositions (Fig. 1B and C). The curve fitting analysis showed good agreement between the measured and calculated data (Fig. 1D).

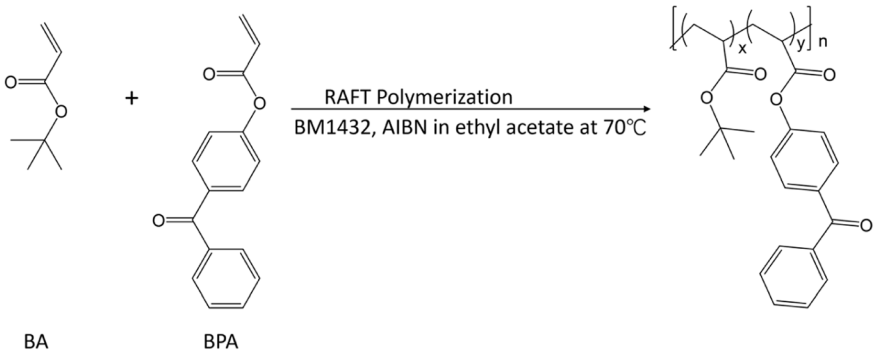

Scheme 2 RAFT copolymerization of BA and BPA.

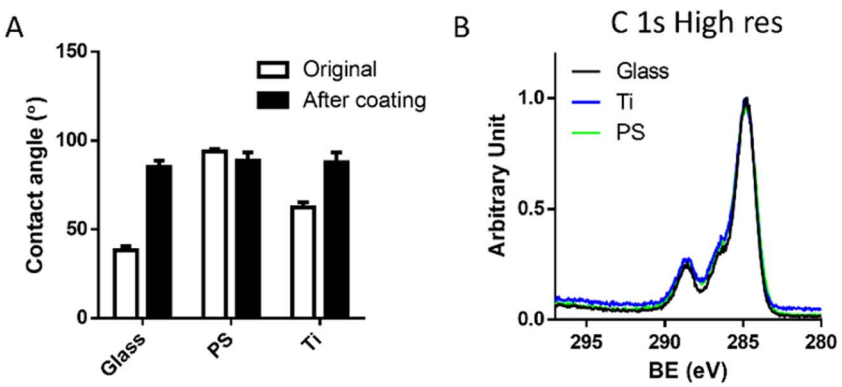

C

	O/C
Glass	0.33 ± 0.02
PS	0.28 ±0.00
Ti	0.36 ± 0.07
Theory	0.29

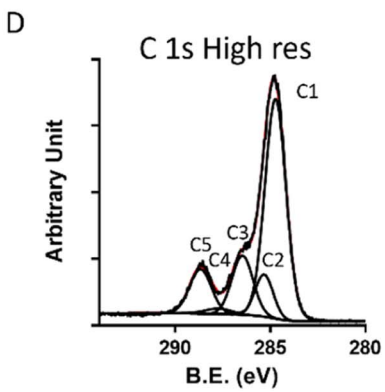

		C1	C2	C3	C4	C5
Position (eV)		284.7	285.3	286.5	287.7	288.7
Component percentage	Measured	69.8		15.9	1.9	12.4
	Calculated	71.9		13.9	0.6	13.6

Fig. 1 (A) Water contact angle (WCA) measurements of different substrates (glass, PS and Ti) with or without BP coating (without UV exposure). (B) High-resolution spectrum of substrates with BP coating (without UV exposure) (black line: glass substrate; blue line: Ti alloy; green line: PS). (C) XPS wide scan for BP polymer coated on glass, PS, and Ti. (D) XPS high-resolution C 1s scan for BP polymer coated glass. For curve fitting of the XPS C 1s high-resolution scans, a 5-component model was applied, where C1 was assigned to C–C and C–H; C2 was assigned to C–N and C–COO (secondary shifts associated with acid and ester groups); C3 was assigned to C–N and C–O; C4 was assigned to R–C═O, O–C–O, and N(H)–C═O and C5 was assigned to O–C═O.

These results indicate that the "glue polymer" was successfully coated on the different substrates.

The consumption of BPA in the polymer was observed using a UV-vis spectrometer. The copolymer was cast on a quartz cuvette. After drying at room temperature, the coating was UV irradiated for 40, 80, 120, 160, and 180 s, respectively. The peak of BPA around 260 nm was significantly dropped after UV irradiation (Fig. 2A). The spectrum between the 160 s and 180 s exposure times were nearly identical, indicating that an irradiation time of 160 s is sufficient to consume the benzophenone (BP) moieties in the copolymers. WCA measurements before and after UV crosslinking revealed that the coating after 160 s irradiation was sufficiently crosslinked to resist ethanol washing (Fig. 2B).

We further characterized the coatings using the Fourier transform infrared spectroscopy (FTIR). The peaks at 1107 cm^{-1}

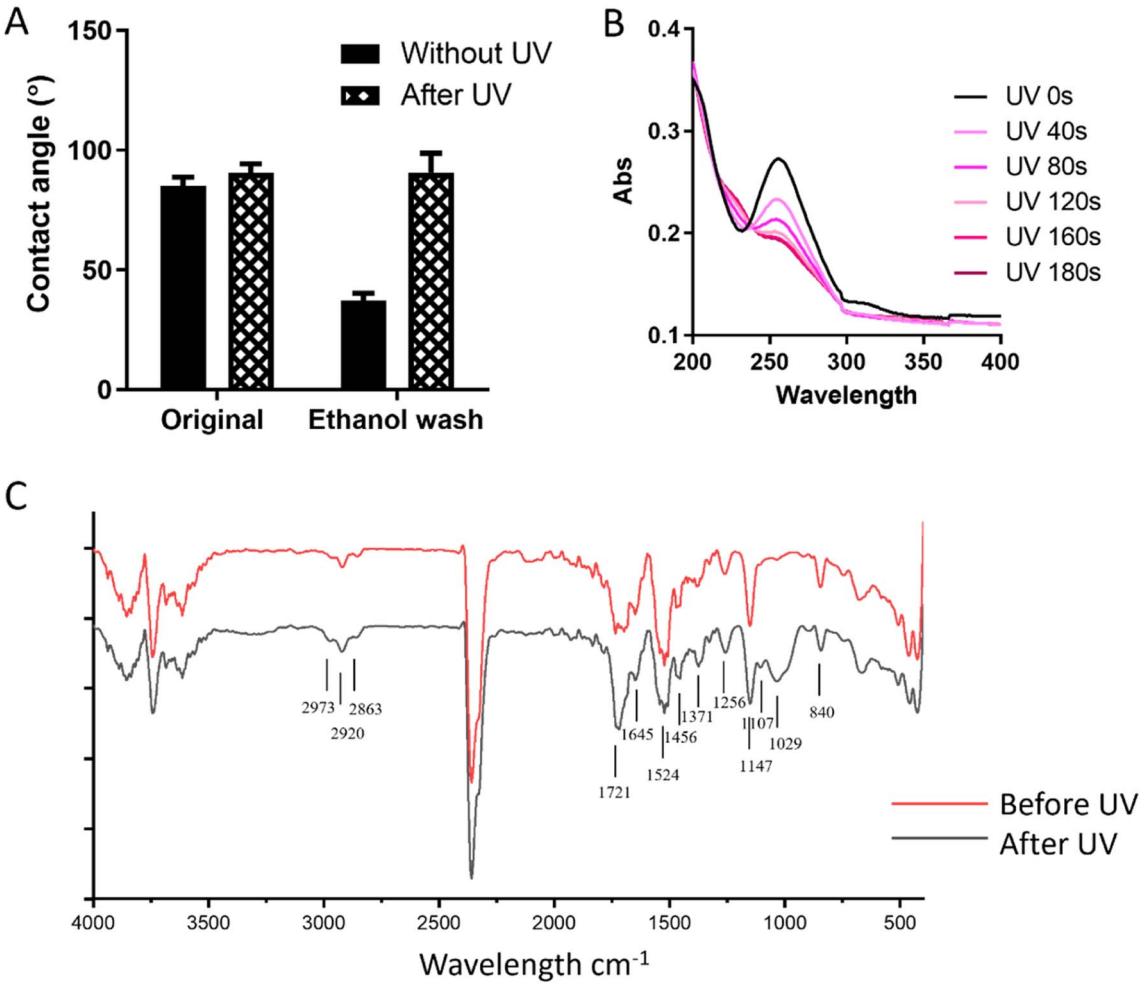

Fig. 2 (A) WCA measurements of a glass substrate coated with BP polymer before and after ethanol wash. (B) UV vis spectrum of BP polymer film with different UV exposure times. (C) FTIR spectrum of BP polymer before (grey line) and after (red line) UV exposure (Ti substrate). Two peaks indicated by the blue arrow were located at 1130 nm and 1023 nm.

and 1029 cm^{-1} appeared after UV irradiation, indicating the generation of C–O and the polymerization of BP groups (Fig. 2C). BP groups were known to form a singlet state, which rapidly undergoes intersystem crossing to yield the triplet by UV excitation. Then, free radicals would be generated *via* the abstraction of hydrogen donors, resulting in a ketyl radical and aliphatic carbon-centred radical. The free radicals can then initiate the crosslink of the coating.[22] The peaks at 2800–3000 cm^{-1} (2973 cm^{-1}, 2920 cm^{-1} and 2863 cm^{-1}) were the C–H stretching from either CH_3 of *tert*-butyl and CH_2 of the polymer backbone (Fig. 2C). The peak at 1721 cm^{-1} is the vibration of ester C=O–O. The bands at 1645 cm^{-1} ascribed to BP's distinctive ketonic C=O group.[23] The peaks at 1524, 1456, and 840 cm^{-1} corresponded to C–C aromatic stretch (in the ring), C–H bending, and ring puckering, respectively.[24]

2.2. Surface functionalization with polyacrylic acid (PAA)

Functionalized surfaces can be generated by simply mixing BP polymer with another functional polymer, such as polyacrylic acid (PAA) (Fig. 3A). A short UV exposure time would be required to increase the ratio of functional groups. For example, pure BP polymer requires 160 s of exposure time, while 20% and 50% PAA require 120 s, and 80% PAA requires only 60 s exposure time (Fig. S2†). FTIR data showed that pure PAA polymer has peaks in 2832–3000, 1709, 1450, 1239, 1169, 915, 801, and 615 cm^{-1} (Fig. 3B). Similarly, the bands between 2832–3000 cm^{-1} were due to the C–H stretching of the polymer backbone. The peaks at 1450 and 1407 cm^{-1} were assigned to the deformation of CH_2 and OH, respectively. The bands between 1110 and 1300 cm^{-1} were contributed by CO stretching and –OH bending vibration. The peak at 615 cm^{-1} was due to the C=O deformation vibration.[25] Peak shown at 1709 cm^{-1} was due to stretching of the carboxylic acid group. In all BP/PAA coatings, FTIR showed distinctive peaks at 840 cm^{-1} of BP and 615/801 cm^{-1} of PAA, indicating a successful crosslinking.

Next, the bioactivity of PAA in the BP/PAA coatings was examined. A scratch was created on the coating, followed by reacting the surface with fluorescent amine (NH_2) *via* EDC/NHS. In the 20% and 50% BP/PAA coatings, a more apparent boundary can be seen on the 50% sample, indicating the

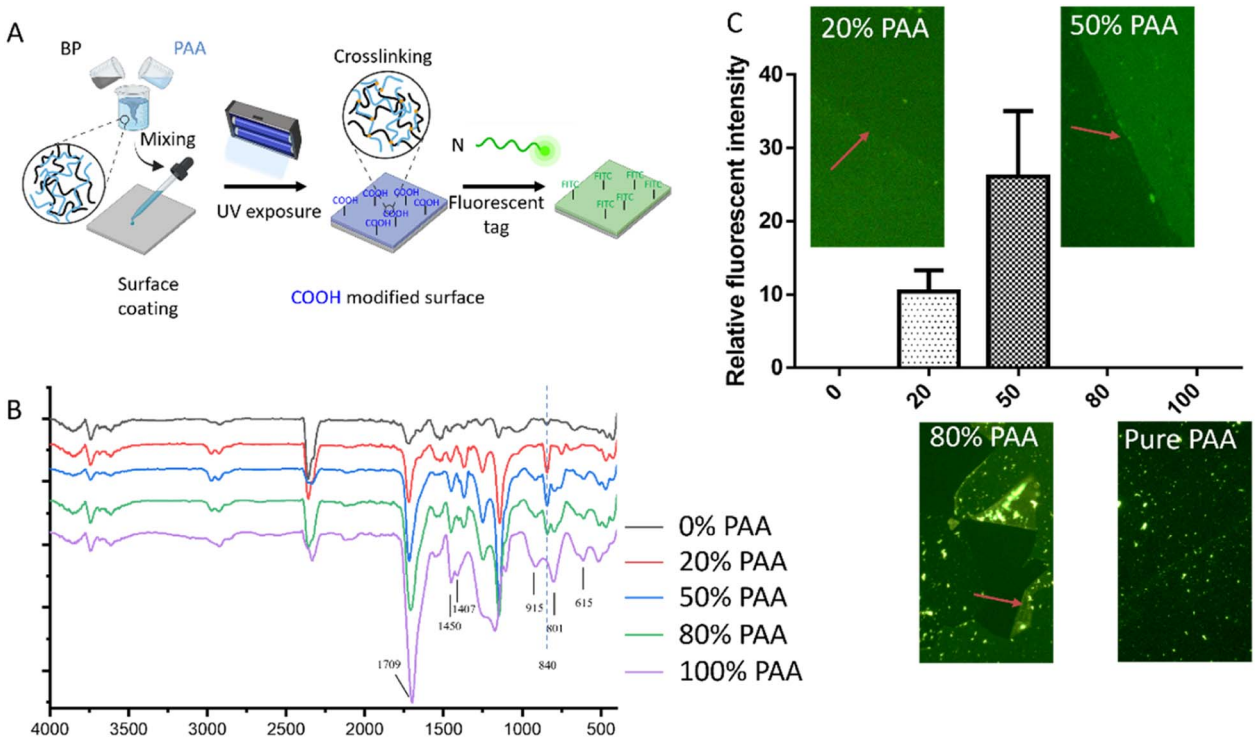

Fig. 3 (A) Schematic drawing of functionalizing surface with carboxylic acid and their further reaction with FITC tag. (B) FTIR spectrum of different BP–PAA polymer coatings after UV exposure. Black line: pure BP; red line: 20% PAA + 80% BP; blue line: 50% PAA + 50% BP; green line: 80% PAA + 20% BP; purple line: pure PAA. (B) UV-vis spectrum of different BP–PAA polymer coatings before (solid lines) and after (dotted lines) UV exposure. (C) Representative images and relative fluorescent intensity on FITC-modified BP–PAA coatings.

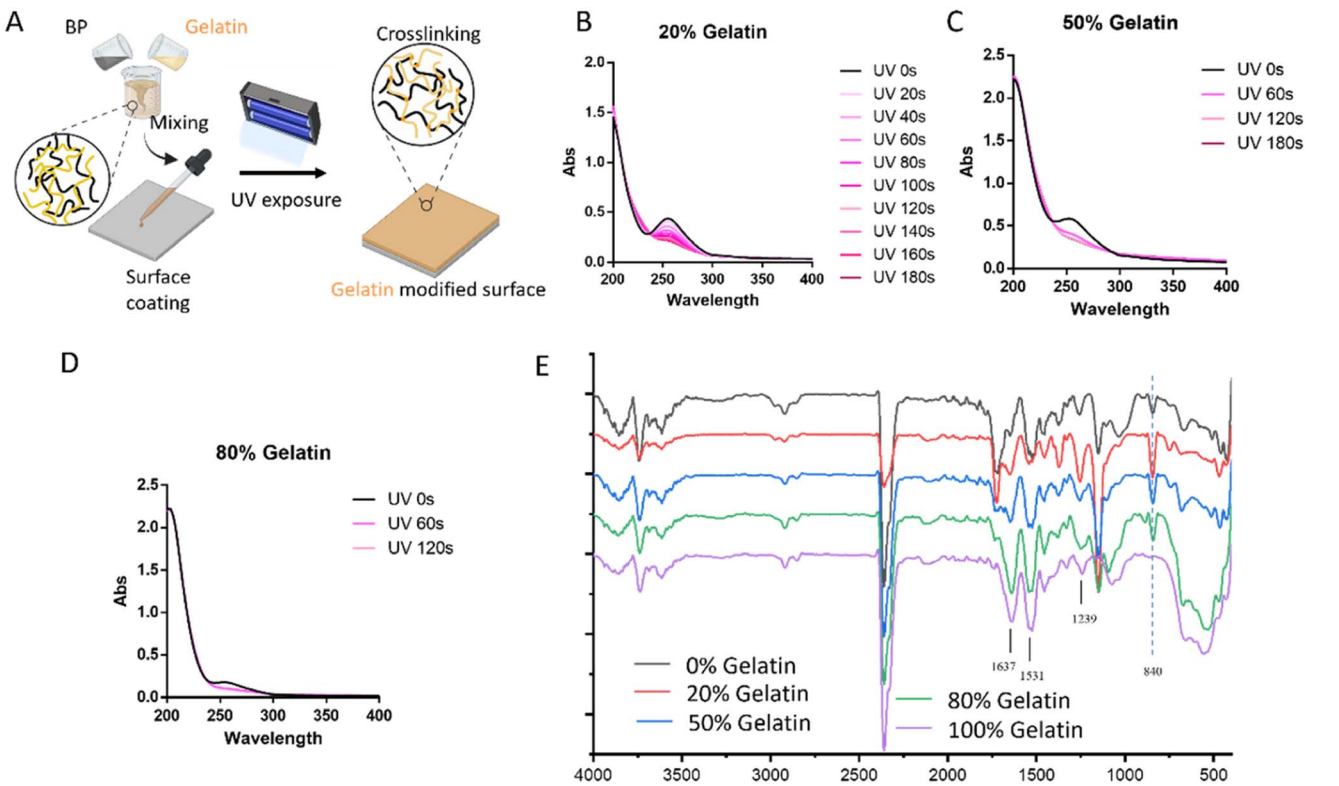

Fig. 4 (A) Schematic drawing of gelatin immobilization method. UV vis spectrum of different BP–gelatin polymer coatings with different UV exposure times. (B) 20% gelatin + 80% BP; (C) 50% gelatin + 50% BP; (D) 80% gelatin + 20% BP. (E) FTIR spectrum of different BP–gelatin polymer coatings after UV exposure. Black line: pure BP; red line: 20% gelatin + 80% BP; blue line: 50% gelatin + 50% BP; green line: 80% gelatin + 20% BP; purple line: pure gelatin.

existing BP/PAA coatings (Fig. 3C). In the 80% PAA coating, delamination was found after sonication. It noted that the BP polymer's reactive points were insufficient. Pure PAA coating control didn't show a fluorescent signal due to its high solubility in water (Fig. 3C).

2.3. Surface functionalization with proteins

Protein-functionalized surfaces can be generated using either one-step (mixing BP with the bioactive molecules) or two-step (sequential coating BP polymer and then the bioactive molecules) methods. For example, gelatin was used in the one-step method. Gelatin was mixed with BP at different ratios (gelatin: 0, 20, 50, 80, and 100%) in solution, and then the mixture was cast on the surfaces (Fig. 4A). A short UV exposure was required for an increased gelatin ratio within the BP/gelatin coating (Fig. 4B–D). FTIR spectrum showed that pure gelatin displayed characteristic peaks at 1637, 1531, and 1239 cm^{-1}, corresponding to amide-I, amide-II, and amide-III, respectively (Fig. 4E).[26] In the one-step method, the characteristic peaks of BP and gelatin co-appeared in the spectrum. In the spectrum of 20%, 50% and 80% gelatin, BP polymer peaks located at 840 and 1720 cm^{-1} appeared with decreased intensity, aligning well with increasing gelatin amount.

Surface bioactivity was evaluated using a cell adhesion study. The pure BP polymer coatings had excellent biocompatibility compared to the tissue culture glass substrate (Fig. 5A and B). To assess the bioactivity of gelatin in the BP/gelatin coatings without interference from adhesive proteins in serum, a 24-hour cell adhesion test was conducted in a serum-free DMEM medium. In the DMEM, NIH 3T3 fibroblasts appeared round-shaped morphology on the glass and BP coating; at the same time, cells were spread out on the BP/gelatin coatings (Fig. 5C). Cell density and activity on the 50% BP/gelatin coating was the highest compared to other surfaces, indicating that an optimal gelatin concentration was found (Fig. 5C). To be noted, cell adhesion was dropped on the BP/gelatin coating (gelatin > 80%) and pure gelatin coating (100%), indicating that gelatin cannot be maintained on the surfaces without enough BP polymer.

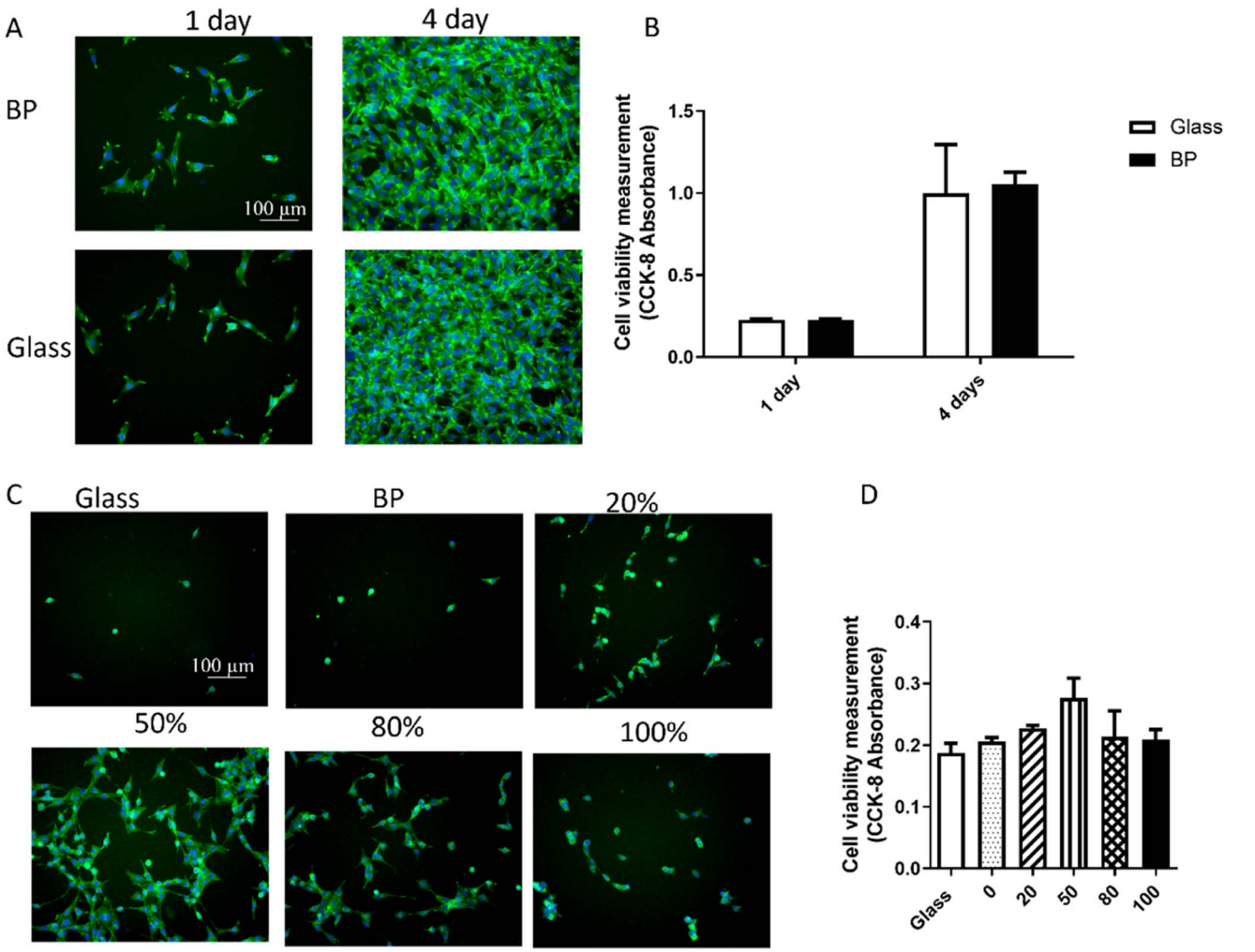

Fig. 5 Representative fluorescent images (A) and cell viability measurement (B) of NIH 3T3 fibroblast culture on BP-coated surfaces and glass control at day 1 and day 4 with complete culture medium. Representative fluorescent images (C) and cell viability measurement (D) of NIH 3T3 cell culture on different BP–gelatin coated surfaces with serum-free culture medium.

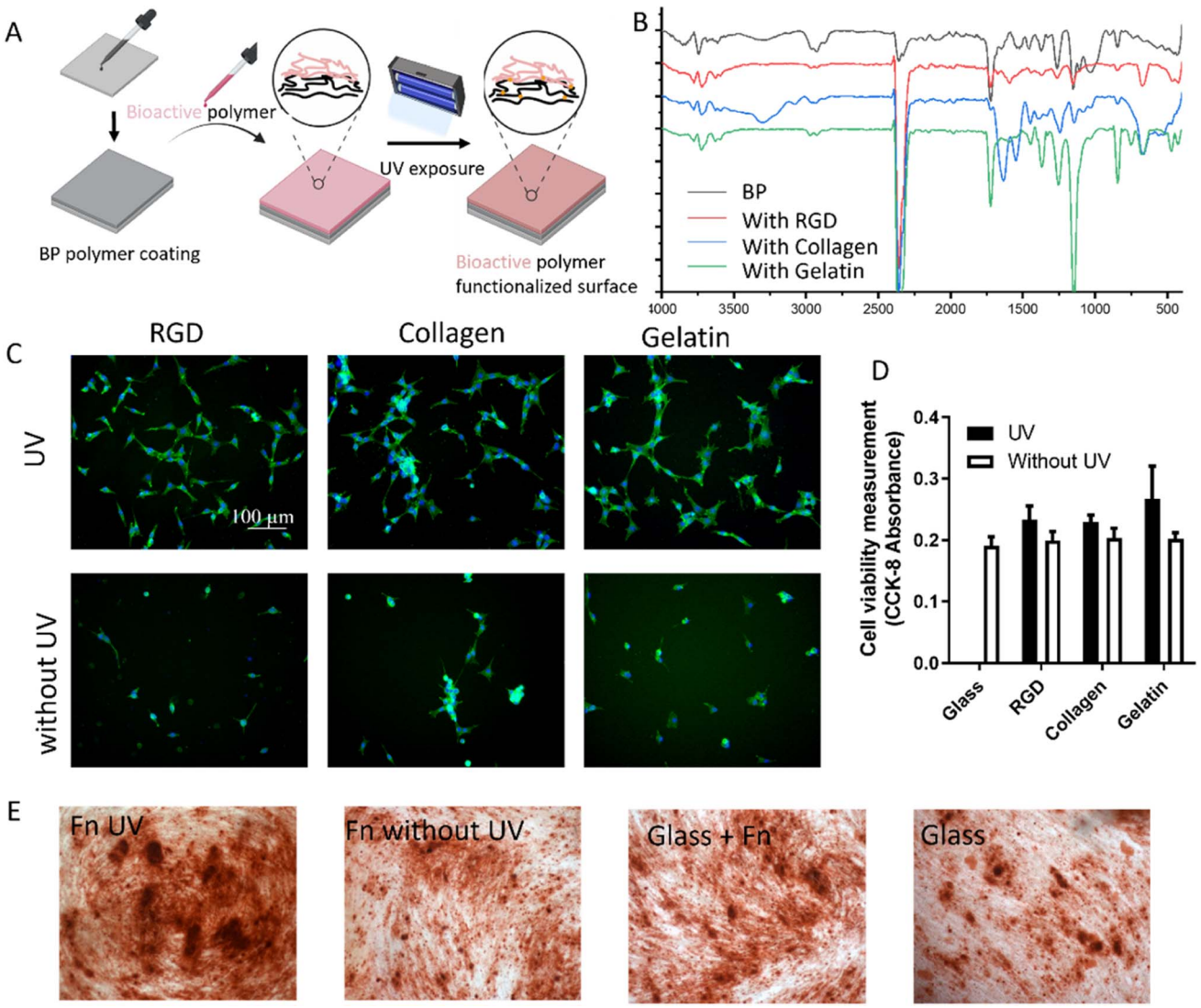

Fig. 6 (A) Schematic drawing of the two-step method for immobilizing bioactive molecules. (B) FTIR spectrum of different bioactive molecule modified surfaces after UV exposure. Black line: pure BP; red line: RGD-coated surface; blue line: collagen-coated surface; green line: gelatin-coated surface. Representative fluorescent images (C) and cell viability measurements (D) of NIH 3T3 cells cultured on RGD, collagen, and gelatin-modified surfaces in a serum-free medium after 24 hours. (E) Representative bright-field images showing ARS staining of calcium deposition after 21 days of hBMSC differentiation culture.

In the two-step method, pure BP polymer was first coated on the surface. After drying, a second layer of bioactive molecules (RGD, collagen, or gelatin) was then cast on the BP film and crosslinked using UV light (Fig. 6A). Since the underneath BP polymer coating retains reactive BP groups, it can chemically bond to the biomolecule cast above. FTIR spectrum confirmed these bioactive polymers attached after washing (Fig. 6B). To evaluate the physical adsorption and UV-crosslinking of proteins within the BP/protein films, NIH 3T3 fibroblasts were cultured on different surfaces with or without UV exposure using serum-free medium. The results showed that UV exposure facilitated cell adhesion without serum, indicating more bioactive molecules on the surfaces (Fig. 6C and D).

The long-term bioactivity of immobilized proteins with BP/protein films was evaluated using fibronectin (FN) and osteogenic differentiation of human bone marrow stem cells (hBMSCs).[27,28] After a 21-day culture under osteogenic differentiation conditions, the highest amount of calcium was produced on the BP/FN film with UV exposure, indicating that the combination of BP polymer and UV crosslinking is necessary (Fig. 6E). The proposed surface coating strategies are beneficial for cell culture and differentiation on biomaterials.

3. Discussion

It has been widely recognized that surface functionalization of a material is crucial in biomaterials and tissue engineering. Substrate-independent coating techniques have gained considerable interest in clinical settings due to their ease of use in coating materials that are otherwise difficult to modify or

require complex reaction steps.[29–31] This study proposes a substrate-independent method using a benzophenone (BP)-containing "glue polymer" and UV-crosslinking. This "glue polymer" is versatile and can be used in one- or two-step coatings. More importantly, the "glue polymer" coatings can be stored in a dry state, which is easy to store and ship. The subsequent UV exposure initiates rapid crosslinking reactions to bind the targeted biomolecules with the surfaces. The bioactivity of the targeted molecules did not harm in either protocol.

This study explores broader applications of BP in biological fields, while BP has been applied in medicine and chemistry (*e.g.*, photo-initiators).[32–34] Borgolte *et al.* synthesized chitosan derivatives substituted with BP groups as antibacterial coatings for polyether ether ketone (PEEK) substrates.[35] Following a similar design concept, Yoshikawa *et al.* embedded BP in a polymer backbone incorporating a low fouling motif and cell adhesive peptide. The resulting coating showed substrate-independent behaviors and antifouling against bacteria.[36] Since BP groups were embedded into the polymer backbone, altering coating properties will require synthesizing new polymers. Moreover, BP molecules can be physically adsorbed onto polydimethylsiloxane (PDMS) surfaces to act as initiators for subsequent crosslinking or grafting. In this setup, surface properties can be modified with different monomers, such as acrylamide, hydroxyethyl methacrylate, and sulfobetaine methacrylate.[37,38] However, the degree of physical adsorption varied on different substrates, potentially leading to inconsistent coatings.

The current method employs BP-containing polymer as a "bioglue", imparting greater stability across different substrates. Targeted molecules can be immobilized onto surfaces without pre-modifications. Additionally, this approach offers the advantages of simplicity in operation and a wide range of candidate polymers, from synthetic polymers to proteins. It does not require specialized equipment with complex parameters, as in plasma polymerization, nor does it need complete submersion of the coated objects. The extensive candidates allow for selecting desired functional groups for immobilization. Water-soluble polymers can be "glued" on the BP-coated surface using the two-step method, wherein BP polymer was dried on the substrates first. Conversely, the mixing method can be adopted if the targeted molecules are only soluble in organic solvents.

The proposed method is an alternative to surface functionalization. The core idea behind this coating technique is the "glue polymer" capable of bonding to a wide range of substrates, ensuring their independence and linking desired functional groups. The BP polymer synthesized serves as a proof of concept, demonstrating how this concept could be applied in biomedical fields.

4. Conclusion

A new substrate-independent coating method employing a benzophenone (BP)-containing "glue polymer" was proposed. This method can be applied to various materials, including glass, PS, and Ti substrates. The "glue polymer" allows efficient UV crosslinking with various biomolecules, including peptides and proteins. Through subsequent cell culture experiments, the sustained bioactivity of these biomolecules was confirmed. This study demonstrates that the proposed method is a versatile and substrate-independent approach. Due to its simplicity, we believe this innovative approach holds significant promise for surface modification in biomedical applications.

5. Experimental section

5.1. Materials

t-Butyl acrylate, AIBN, ethyl acetate, methanol, polyacrylic acid (PAA), hexafluoroisopropanol paraformaldehyde, Triton-100, β-glycerophosphate, dexamethasone and ascorbic acid were purchased from Sigma and used as received without further purification. Gelatin (from porcine skin) were purchased from Milliporesigma. Collagen IV (mice) were purchased from Corning. *N*-Benzophenone acrylate (BPA) and BM1432 (RAFT agent) were donated from Paul Pasic. FITC–RGD with amine as the end group was purchased from BioMATIK (Lot#: P130801, Taiwan). Dulbecco's modified Eagle medium (DMEM), fetal bovine serum (FBS), MEM-a medium (PM150421), penicillin and streptomycin solution were all purchased from Gibico. CCK-8 kits were purchased from Dojindo Molecular Technologies. cRGD were purchased from Qyaobio, China. Fibronectin was purchased from Stem Cell Technology.

5.2. BP polymer synthesis

Copolymerization of BPA and BA (poly(BA_{95}–BPA_5)). 5BPA–BA: 3 g *t*-butyl acrylate (BA, 3 g, 24 mmol), *N*-benzophenone acrylate (BPA, 305 mg, 0.12 mmol), RAFT reagent BM1432 (48 mg, 0.12 mmol) and AIBN (1.9 mg, 0.01 mmol) were prepared in a N_2 purged glove box. Then, they were dissolved in 20 mL N_2 purged ethyl acetate and continued to purge for 10 minutes within the glove box. The reaction was carried out at 70 °C for 20 h. The polymer was precipitated into a methanol/water (30/70 volume ratio) mixture and dried in a vacuum. The number-average molecular weight (M_n) and polydispersity (M_w/M_n) were measured by gel permeation chromatography (GPC) using a Shimadzu Chromatography System (LC-24AD) with Ultrahydrogel 2000 and 120 columns connected in series. The molar ratio of BPA and HPA in the copolymer was determined by ^{1}H NMR.

5.3. Coating preparation

For pre-mixed coatings: BP polymers were pre-mixed with either PAA (in acetic acid) or gelatin (in hexafluoroisopropanol) at a pre-determined ratio and diluted to a final solution containing 2 wt% of polymer solutes. These solutions were spin-coated on different substrates (2700 rpm for 25 s), including cover glass, Ti alloy and PS pallet.

For the post-coating method, BP–RGD coating is an example. 2 wt% of BP polymer in toluene was spin-coated on a substrate (2700 rpm for 25 s) first. 100 μL (0.01 mg mL^{-1}) cRGD water solution was dropped onto the surface and restrained in a Ø

1 cm area with a silicon O ring. After drying overnight, the surface was crosslinked and washed with 1% Twin-20 form 16 h under gentle shaking to remove the physically attached cRGD. The samples were then washed thoroughly with MQ water before further use. For BP–gelatin and BP–collagen coatings, 0.1 mg mL^{-1} coating solution (in MQ water) was used instead, followed by the same drying, crosslinking and washing processes (without Twin-20 washing). Crosslinking method: coatings were crosslinked under a portable UV lamp (Yihua Lighting Company, China) containing UV-A, UV-B and UV-C for a predetermined time. The distance between the lamp and the crosslinking surface remains 10 cm for all experiments.

5.4. Coating characterization

UV-vis spectrum. 10 μL polymer solution was casted on one side of a 3 mL quartz cuvette (Agilent Technology) and allowed to dry overnight in the dark. UV-vis spectrum spectra were recorded in Cary 60 UV-vis spectrophotometer at a nominal resolution of 2 nm with 600 nm min^{-1} scan rate. All measurements were performed at room temperature.

X-ray photoelectron spectroscopy (XPS). XPS was performed on ESCALAB 250Xi spectrometer (Thermo Fisher Scientific Inc.), equipped with a monochromatized Al Kα source at a power of 150 W (15 kV), a hemispherical analyzer operating in the fixed analyzer transmission mode, and the standard aperture with an analysis area of 0.5 mm × 0.5 mm. The total pressure, in the order of 10^{-10} mbar, was maintained in the main vacuum chamber during analysis. Survey spectra were acquired at 100 eV pass energy, and high-resolution C 1s, N 1s and O 1s spectra were obtained at pass energy of 20 eV. Data were processed with Thermo Avantage software. All elements present were identified from survey spectra. The atomic concentrations of the detected elements were calculated using integral peak intensities and the sensitivity factors supplied by the manufacturer. All spectra were calibrated according to C 1s located at 284.8 eV. For curve fitting of the XPS C 1s high-resolution scans, a 5-component model was applied, where C1 was assigned to C–C, C–H and C–S; C2 was assigned to C–Br, C–N and C–COO (secondary shifts associated with acid and ester groups); C3 was assigned to C–N and C–O; C4 was assigned to R–C=O, O–C–O and N(H)–C=O and C5 was assigned to O–C=O.

Water contact angle. The static contact angle of the surfaces was calculated and measured using the sessile drop method with a 3 μL water droplet on a DataPhysics Instrument (OCA20) at ambient temperature using MQ water.

Fourier transfer infrared spectroscopy (FTIR) measurements were performed on a Nicolet 6700 ATR-FTIR spectrometer using XT-KBr™ beam splitters with a SMART SAGA attachment and a grazing angle of 80°. Spectra were recorded at 4 cm^{-1} resolution of 128 scans with a spectral range of 4000–500 cm^{-1}.

Cell culture. NIH 3T3 fibroblasts and human fetal bone marrow stem cells (BMSCs) were used in this study. NIH 3T3 cells were cultivated in complete culture media (composed of Dulbecco's modified Eagle medium (DMEM) containing 10% FBS, 100 units per mL penicillin and 100 μg per mL streptomycin (antibiotics)) at 37 °C using a 5% CO_2 incubator for maintenance and passaged once cell density reached 80–90% confluency. hBMSCs were maintained in growth media (GM, MEM-a medium (PM150421) supplemented with 10% FBS and 100 units per mL penicillin and 100 μg per mL streptomycin) and used before passage 10. For biocompatibility culture, samples were placed at the bottom of a 24-well plate and sterilized by soaking in 75% ethanol for 30 min and dried in a biosafety cabinet overnight. NIH 3T3 cells were seeded onto the samples at a density of 5000 cells per well in 0.8 mL of complete culture media for a predetermined time. In the cell adhesive assay, samples were sterilized by soaking in 1000 units per mL penicillin and 1 mg per mL streptomycin at room temperature for 16 h and then washed with sterile PBS thoroughly before cell seeding. NIH 3T3 cells were seeded at the density of 10 000 cells per well in 0.5 mL DMEM media (the serum-free medium without the addition of FBS) with 100 units per mL penicillin and 100 μg per mL streptomycin for 24 h.

Cell attachment measurement. Cell viability was investigated using a Cell Counting Kit-8 assay (CCK-8, Dojindo Molecular Technologies). For fluorescence imaging, cells were fixed using 4% paraformaldehyde for 10 min at room temperature after being carefully washed in sterile PBS and then permeabilized with 0.2% Triton X-100 for another 10 min. Cell skeleton staining was performed by incubating cells with phalloidin (Alexa Fluor 488, Thermofisher; 1 : 200) for 30 min at room temperature and rinsing with PBS. Images were taken under a fluorescent microscope (Olympus CKX53).

Osteogenesis differentiation. For long-term cell culture, BMSCs were seeded at near-confluent densities (20 000 cells per cm^2). Once the cell density reached about 90%, the medium was changed to an osteogenic medium and further incubated. The osteogenic supplements included a growth medium containing 10 mM β-glycerophosphate, (Sigma-Aldrich, G9422-10G), 10^{-7} M dexamethasone (Sigma-Aldrich, D8893-1MG), and 50 μg per mL L-ascorbic acid (Sigma-Aldrich, A8960-5G).

Alizarin red S (ARS) staining. After 21 days of differentiation, the cells were washed twice with PBS, fixed with 4% paraformaldehyde for 10 minutes, and incubated with 0.1% alizarin red S solution for 30 minutes. The deposition of calcium phosphate was indicated by red staining.

Author contributions

PYW and HT conceived and supervised this study. YS, XT, and PD conducted the experiments. PP and LE helped with the experimental procedures. YS, HT, and PYW wrote and revised the manuscript. All authors have approved the final version of the manuscript.

Conflicts of interest

The authors declare no competing interests.

Acknowledgements

PYW thanks the support from the Ministry of Science and Technology of China (2022YFA1105101); the Chinese Academy

of Sciences (172644KYSB20200002 and 172644KYSB20200048); Zhejiang Provincial Natural Science Foundation of China (LZ23C070004). BioRender was used to create schematic images.

References

1 P. Y. Wang, L. R. Clements, H. Thissen, W. B. Tsai and N. H. Voelcker, Screening rat mesenchymal stem cell attachment and differentiation on surface chemistries using plasma polymer gradients, *Acta Biomater.*, 2015, **11**, 58–67, DOI: **10.1016/j.actbio.2014.09.027**.

2 Y.-C. Liu, J.-W. Jhang, K. Liu, H. Pan, H.-Y. Chen and P.-Y. Wang, Hybrid Surface Nanostructures Using Chemical Vapor Deposition and Colloidal Self-Assembled Patterns for Human Mesenchymal Stem Cell Culture—A Preliminary Study, *Coatings*, 2022, **12**(3), 311, DOI: **10.3390/coatings12030311**.

3 Y. Shi, K. Liu, Z. Zhang, X. Tao, H.-Y. Chen, P. Kingshott and P.-Y. Wang, Decoration of Material Surfaces with Complex Physicochemical Signals for Biointerface Applications, *ACS Biomater. Sci. Eng.*, 2020, **6**(4), 1836–1851, DOI: **10.1021/acsbiomaterials.9b01806**.

4 N. R. Barros, Y. Chen, V. Hosseini, W. Wang, R. Nasiri, M. Mahmoodi, E. P. Yalcintas, R. Haghniaz, M. M. Mecwan, S. Karamikamkar, *et al.*, Recent developments in mussel-inspired materials for biomedical applications, *Biomater. Sci.*, 2021, **9**(20), 6653–6672, DOI: **10.1039/D1BM01126J**.

5 J. Harati, X. Tao, H. Shahsavarani, P. Du, M. Galluzzi, K. Liu, Z. Zhang, P. Shaw, M. A. Shokrgozar, H. Pan and P. Y. Wang, Polydopamine-Mediated Protein Adsorption Alters the Epigenetic Status and Differentiation of Primary Human Adipose-Derived Stem Cells (HASCs), *Front. bioeng. biotechnol.*, 2022, **10**, 934179, DOI: **10.3389/fbioe.2022.934179**.

6 S. El Yakhlifi and V. Ball, Polydopamine as a stable and functional nanomaterial, *Colloids Surf., B*, 2020, **186**, 110719, DOI: **10.1016/j.colsurfb.2019.110719**.

7 Q. Huang, J. Chen, M. Liu, H. Huang, X. Zhang and Y. Wei, Polydopamine-based functional materials and their applications in energy, environmental, and catalytic fields: state-of-the-art review, *Chem. Eng. J.*, 2020, **387**, 124019, DOI: **10.1016/j.cej.2020.124019**.

8 H. Li, D. Yin, W. Li, Q. Tang, L. Zou and Q. Peng, Polydopamine-based nanomaterials and their potentials in advanced drug delivery and therapy, *Colloids Surf., B*, 2021, **199**, 111502, DOI: **10.1016/j.colsurfb.2020.111502**.

9 W. Cheng, X. Zeng, H. Chen, Z. Li, W. Zeng, L. Mei and Y. Zhao, Versatile Polydopamine Platforms: Synthesis and Promising Applications for Surface Modification and Advanced Nanomedicine, *ACS Nano*, 2019, **13**(8), 8537–8565, DOI: **10.1021/acsnano.9b04436**.

10 M. Farokhi, F. Mottaghitalab, M. R. Saeb and S. Thomas, Functionalized theranostic nanocarriers with bio-inspired polydopamine for tumor imaging and chemo-photothermal therapy, *J. Controlled Release*, 2019, **309**, 203–219, DOI: **10.1016/j.jconrel.2019.07.036**.

11 H. Tolabi, N. Bakhtiary, S. Sayadi, M. Tamaddon, F. Ghorbani, A. R. Boccaccini and C. Liu, A critical review on polydopamine surface-modified scaffolds in musculoskeletal regeneration, *Front. Bioeng. Biotechnol.*, 2022, **10**, 1008360, DOI: **10.3389/fbioe.2022.1008360**.

12 H. Choi and K. Lee, Crosslinking Mechanisms of Phenol, Catechol, and Gallol for Synthetic Polyphenols: A Comparative Review, *Appl. Sci.*, 2022, **12**(22), 11626, DOI: **10.3390/app122211626**.

13 L. Yang, Y. Zou, W. Xia, H. Li, X. He, Y. Zhou, X. Liu, C. Zhang and Y. Li, Tea stain-inspired solar energy harvesting polyphenolic nanocoatings with tunable absorption spectra, *Nano Res.*, 2021, **14**(4), 969–975, DOI: **10.1007/s12274-020-3134-9**.

14 X. Zhang, Z. Li, P. Yang, G. Duan, X. Liu, Z. Gu and Y. Li, Polyphenol scaffolds in tissue engineering, *Mater. Horiz.*, 2021, **8**(1), 145–167, DOI: **10.1039/D0MH01317J**.

15 H. Thissen, A. Koegler, M. Salwiczek, C. D. Easton, Y. Qu, T. Lithgow and R. A. Evans, Prebiotic-chemistry inspired polymer coatings for biomedical and material science applications, *NPG Asia Mater.*, 2015, **7**(11), e225, DOI: **10.1038/am.2015.122**.

16 R. J. Toh, R. Evans, H. Thissen, N. H. Voelcker, M. d'Ischia and V. Ball, Deposition of Aminomalononitrile-Based Films: Kinetics, Chemistry, and Morphology, *Langmuir*, 2019, **35**(30), 9896–9903, DOI: **10.1021/acs.langmuir.9b01497**.

17 H. Thissen, R. A. Evans and V. Ball, Films and Materials Derived from Aminomalononitrile, *Processes*, 2021, **9**(1), 82, DOI: **10.3390/pr9010082**.

18 T.-Y. Liao, C. D. Easton, H. Thissen and W.-B. Tsai, Aminomalononitrile-Assisted Multifunctional Antibacterial Coatings, *ACS Biomater. Sci. Eng.*, 2020, **6**(6), 3349–3360, DOI: **10.1021/acsbiomaterials.0c00148**.

19 W.-H. Chen, T.-Y. Liao, H. Thissen and W.-B. Tsai, One-Step Aminomalononitrile-Based Coatings Containing Zwitterionic Copolymers for the Reduction of Biofouling and the Foreign Body Response, *ACS Biomater. Sci. Eng.*, 2019, **5**(12), 6454–6462, DOI: **10.1021/acsbiomaterials.9b00871**.

20 D. J. Menzies, A. Ang, H. Thissen and R. A. Evans, Adhesive Prebiotic Chemistry Inspired Coatings for Bone Contacting Applications, *ACS Biomater. Sci. Eng.*, 2017, **3**(5), 793–806, DOI: **10.1021/acsbiomaterials.7b00038**.

21 C.-Y. Wu, Y.-C. Chiang, J. Christy, A. P.-H. Huang, N.-Y. Chang, Wenny, Y.-C. Chiu, Y.-C. Yang, P.-C. Chen, P.-Y. Wang, *et al.*, Guiding Stem Cell Differentiation and Proliferation Activities Based on Nanometer-Thick Functionalized Poly-p-xylylene Coatings, *Coatings*, 2021, **11**(5), 582, DOI: **10.3390/coatings11050582**.

22 S. K. Christensen, M. C. Chiappelli and R. C. Hayward, Gelation of Copolymers with Pendent Benzophenone Photo-Cross-Linkers, *Macromolecules*, 2012, **45**(12), 5237–5246, DOI: **10.1021/ma300784d**.

23 I. Juchnovski, T. Kolev and B. Stamboliyska, Infrared Spectra of Benzophenone-Ketyls. Effects of Meta- and Para-Substituents on the vC[dbnd]O Frequencies. Correlation Of vC[dbnd]O Of Substituted Benzophenone-ketyls With The Hueckel PC[dbnd]O Bond Order, *Spectrosc. Lett.*, 1993, **26**(1), 67–78, DOI: **10.1080/00387019308011515**.

24 M. C. Tria, J. Y. Park and R. Advincula, Electrochemically-deposited benzophenone moieties: precursors for dual mode patterning of polymer brushes on conducting surfaces, *Chem. Commun.*, 2011, **47**(8), 2393–2395, DOI: **10.1039/C0CC04046K**.

25 M. Todică, R. Stefan, C. V. Pop and L. E. Olar, IR and Raman Investigation of Some Poly(acrylic) Acid Gels in Aqueous and Neutralized State, *Acta Phys. Pol., A*, 2015, **128**, 128–135, DOI: **10.12693/APhysPolA.128.128**.

26 S. Roy and J.-W. Rhim, Preparation of antimicrobial and antioxidant gelatin/curcumin composite films for active food packaging application, *Colloids Surf., B*, 2020, **188**, 110761, DOI: **10.1016/j.colsurfb.2019.110761**.

27 J. Klavert and B. C. J. van der Eerden, Fibronectin in Fracture Healing: Biological Mechanisms and Regenerative Avenues, *Front. Bioeng. Biotechnol.*, 2021, **9**, 663357, DOI: **10.3389/fbioe.2021.663357**.

28 A. B. Faia-Torres, T. Goren, T. O. Ihalainen, S. Guimond-Lischer, M. Charnley, M. Rottmar, K. Maniura-Weber, N. D. Spencer, R. L. Reis, M. Textor, *et al.*, Regulation of Human Mesenchymal Stem Cell Osteogenesis by Specific Surface Density of Fibronectin: a Gradient Study, *ACS Appl. Mater. Interfaces*, 2015, **7**(4), 2367–2375, DOI: **10.1021/am506951c**.

29 M. K. Shave, Y. Zhou, J. Kim, Y. C. Kim, J. Hutchison, D. Bendejacq, M. Goulian, J. Choi, R. J. Composto and D. Lee, Zwitterionic surface chemistry enhances detachment of bacteria under shear, *Soft Matter*, 2022, **18**(35), 6618–6628, DOI: **10.1039/D2SM00065B**.

30 I. Çaha, A. C. Alves, L. A. Rocha and F. Toptan, A Review on Bio-functionalization of β-Ti Alloys, *J. Bio- Tribo-Corros.*, 2020, **6**(4), 135, DOI: **10.1007/s40735-020-00432-0**.

31 T. Egghe, R. Morent, R. Hoogenboom and N. De Geyter, Substrate-independent and widely applicable deposition of antibacterial coatings, *Trends Biotechnol.*, 2023, **41**(1), 63–76, DOI: **10.1016/j.tibtech.2022.06.003**.

32 K. Surana, B. Chaudhary, M. Diwaker and S. Sharma, Benzophenone: a ubiquitous scaffold in medicinal chemistry, *MedChemComm*, 2018, **9**(11), 1803–1817, DOI: **10.1039/C8MD00300A**.

33 A. Kowalska, J. Sokolowski and K. Bociong, The Photoinitiators Used in Resin Based Dental Composite-A Review and Future Perspectives, *Polymers*, 2021, **13**(3), 470, DOI: **10.3390/polym13030470**.

34 S. Liu, D. Brunel, G. Noirbent, A. Mau, H. Chen, F. Morlet-Savary, B. Graff, D. Gigmes, P. Xiao, F. Dumur, *et al.*, New multifunctional benzophenone-based photoinitiators with high migration stability and their applications in 3D printing, *Mater. Chem. Front.*, 2021, **5**(4), 1982–1994, DOI: **10.1039/D0QM00885K**.

35 M. Borgolte, O. Riester, I. Quint, F. Blendinger, V. Bucher, S. Laufer, R. Csuk, L. Scotti and H. P. Deigner, Synthesis of a biocompatible benzophenone-substituted chitosan hydrogel as novel coating for PEEK with extraordinary strong antibacterial and anti-biofilm properties, *Mater. Today Chem.*, 2022, **26**, 101176, DOI: **10.1016/j.mtchem.2022.101176**.

36 C. Yoshikawa, T. Nakaji-Hirabayashi, N. Nishijima, P. Nonsuwan, R. J. Toh, W. Kowalczyk and H. Thissen, Ultra-low fouling photocrosslinked coatings for the selective capture of cells expressing CD44, *Mater. Sci. Eng., C*, 2021, **120**, 111630, DOI: **10.1016/j.msec.2020.111630**.

37 D. Keskin, T. Mokabbar, Y. Pei and P. Van Rijn, The Relationship between Bulk Silicone and Benzophenone-Initiated Hydrogel Coating Properties, *Polymers*, 2018, **10**(5), 534, DOI: **10.3390/polym10050534**.

38 B. L. Leigh, E. Cheng, L. Xu, A. Derk, M. R. Hansen and C. A. Guymon, Antifouling Photograftable Zwitterionic Coatings on PDMS Substrates, *Langmuir*, 2019, **35**(5), 1100–1110, DOI: **10.1021/acs.langmuir.8b00838**.